Journal of Solid State Chemistry **152,** 546–553 (2000)
doi:10.1006/jssc.2000.8729, available online at http://www.idealibrary.com on IDEAL®

Structural Characterization of the Engineered Scavenger Compound, H-$Li_2Ti_3O_7$

P. Bordet,* C. Bougerol Chaillout,* I. E. Grey,†,[1] J. L. Hodeau,* and O. Isnard*

* *CNRS Laboratoire de Cristallographie, BP166, 38042 Grenoble, France; and † CSIRO Minerals, Box 312, Clayton South, Australia 3169*

Received January 19, 2000; in revised form March 20, 2000; accepted March 27, 2000

The so-called H phase in the system Li_2O–TiO_2 was prepared from niobia-doped R-$Li_2Ti_3O_7$ (ramsdellite form) by reheating the quenched metastable R phase to 1000 K. The phase was characterized using transmission electron microscopy (TEM), powder X-ray diffraction (XRD), and powder neutron diffraction (ND). It has trigonal symmetry, space group $R\bar{3}c$, with hexagonal cell parameters $a = 5.0744(1)$ Å and $c = 69.9405(3)$ Å at 303 K. The unit cell composition is $Li_{28.5}Ti_{36.5}Nb_{1.1}O_{90}$. High-resolution TEM images were used to establish a starting model for the structure, which was refined by the Rietveld method using ND data collected at 1.5 K, to $R_{wp} = 5.8\%$, $R_B = 2.0\%$ (350 reflections). The structure comprises an ordered intergrowth, parallel to (001) of blocks of corundum-type $[Ti_2O_3]^{2+}$ and $LiNbO_3$-type structures. The Li atoms in the centre of the $LiNbO_3$-type blocks have triangular coordination as in paraelectric $LiNbO_3$. The effect of temperature on the structure was studied by Rietveld refinement of XRD data sets collected between 100 and 1173 K. The relationship to the structure of the R phase is discussed. © 2000 Academic Press

INTRODUCTION

A phase with composition close to $Li_2Ti_3O_7$ in the pseudobinary phase diagram Li_2O–TiO_2 was first reported by Jonker (1). The phase was proposed to have a ramsdellite (R)-type structure by Lundberg and Andersson (2). This was confirmed in a single-crystal X-ray study by Morosin and Mikkelsen (3). Based on the structure refinement the formula is more correctly written as $Li_{1.72}[Li_{0.57}Ti_{3.43}]O_8$, in which part of the lithium substitutes for titanium in the octahedral framework as originally proposed by Roth *et al.* (4).

Subsequent investigations of the pseudobinary phase system (5, 6) showed that at temperatures below 1213 K, $Li_2Ti_3O_7$ (R) is unstable relative to a mixture of $Li_4Ti_5O_{12}$ (spinel) and rutile. The R phase could be preserved metastably by quenching. Mikkelsen (6) observed that on reheating the quenched R phase at ~700–900 K it transformed into a new phase for which the X-ray diffraction (XRD) patterns could be indexed using a hexagonal (H) cell with $a = 8.78$ Å and $c = 69.86$ Å. A transmission electron microscopy (TEM) study on the H phase by Zou *et al.* (7) revealed the presence of two separate phases which were labeled H1 and H2, both belonging to the trigonal system. The phase H1, with space group $R3c$ or $R\bar{3}c$ had hexagonal cell parameters $a = 5.14$ Å ($\sim 8.78/\sqrt{3}$), $c = 70.2$ Å, related to those given by Mikkelsen (6). The phase H2 had a primitive trigonal cell with $a = 5.14$ Å and $c = 9.36$ Å. Coherent intergrowth of H1 and H2 along [001] was commonly observed.

The transformation of the R to the H phase was investigated by Tsubone and Shimizu (8). In the pseudobinary system the phase transition R → H occurred at 900 K and was accompanied by a partial decomposition of H to spinel plus rutile. Tsubone and Shimizu found that addition of small amounts (3–5 mol %) of Nb_2O_5 facilitated the R → H phase transition and suppressed the consecutive decomposition reaction, giving an almost pure H phase product. The niobia addition also stabilised the H phase to higher temperatures. The powder XRD pattern of the phase containing 3 mol% niobia was indexed using cell parameters $a = 8.778(8)$ Å and $c = 69.88(2)$ Å, related to those of the H1 phase (7).

Recently, $Li_2Ti_3O_7$ gained commercial interest as an Engineered Scavenger Compound, ESC, (9) because of its ability to selectively recover lithium from aluminum–lithium scrap alloys. Studies on the scavenging process have shown that electrochemical loading of lithium into the R phase at 873 K causes a rapid transformation to the H phase. The H phase was reported to be as effective a scavenger as the R phase (9). However, the scavenging mechanism remained unclear as the structure of the H phase had not been determined. We report here the preparation of the H1 phase stabilized by niobia addition and a determination and refinement of its crystal structure using a combination of high-resolution TEM, powder XRD, and neutron diffraction.

[1] To whom proofs should be sent. E-mail: ian.grey@minerals.csiro.au.

0022-4596/00 $35.00

EXPERIMENTAL PROCEDURES

Synthesis

A mixture of high-purity starting materials of Li_2CO_3, TiO_2, and Nb_2O_5, in the molar ratio 0.96 : 2.69 : 0.04, was intimately ground, pelleted, and preheated in a platinum crucible to 1173 K to decompose the carbonate. The sample was reground, pelleted, and heated in air to 1500 K for 24 h and then cooled by removing from the furnace. A powder XRD pattern showed that the product was single-phase R-type. After fine grinding in methanol, the repelleted sample was heated from ambient to 773 K at 50 K/h, held for 1 h, heated to 1000 K at 20 K/h, held for 1 h, and then removed from the furnace. A powder XRD pattern showed a well-crystallized product with a small amount of rutile as the only impurity.

Diffraction Studies

Electron diffraction/microscopy studies were made using a Philips CM300 transmission electron microscope operated at 300 kV, with a C_s coefficient of 1.2 mm. Studies were made on thin edges of crystals produced by fracturing.

Routine phase identification was made using a Siemens D5000 powder diffractometer operated in transmission mode. Data collections for structure refinement were obtained at the European Synchrotron Radiation Facility using the high-resolution multi-detector powder diffractometer on beam line BM16 (10). The finely ground sample was packed in a 1-mm quartz capillary which was spun about the axis of the diffractometer to minimize the effect of preferred orientation. A wavelength of 0.44535 Å was employed. Data sets were collected at 100, 300, 473, 673, 873, 1073, and 1173 K. The different temperatures were achieved by passing a stream of cold or hot gas over the capillary.

A neutron diffraction (ND) data set was obtained at a temperature of 1.5 K on the high-resolution powder diffractometer D2B (11) at the Institut Laue Langevin. Data in the 2θ range of 2–160° were collected using a wavength of 1.594 Å (selected by the (335) reflection of a Ge monochromator) and a step width of 0.05°.

Refinements

Least-squares refinements were made using the Rietveld programs SR5, a local modification of the code by Hill and Howard (12), Wiles and Young (13), and FULLPROF (14). A pseudo-Voigt peak shape function was employed, together with a three-term full-width at half-maximum function (15) and a four-parameter polynomial for the background.

RESULTS AND DISCUSSION

TEM Studies

Selected area electron diffraction patterns could all be indexed on the basis of the H1 cell reported by Zou *et al.* (7) with $a = 5.07$ Å and $c = 69.9$ Å. In fact the diffraction data reported by Mikkelsen (6) can also be fully indexed using these cell parameters in place of the larger cell with $a = 8.78 = \sqrt{3} \times 5.07$ Å that he used. Different zones were obtained by rotation about c^*. The observed systematic absences established the possible space groups as $R3c$ or $R\bar{3}c$, as found by Zou *et al.* (7). We found no evidence for the H2 phase observed by Zou *et al.* (7). Consistent with this, Tsubone and Shimizu (8) were able to completely index powder XRD patterns of niobia-doped H phase using the H1 cell, which suggests that the niobia doping stabilizes the H1 phase relative to H2.

A typical high-resolution electron image obtained near the edge of a thin crystallite (projected along [110]) is shown in Fig. 1. It bears a close resemblance to the corresponding image presented by Zou *et al.* for their H1 phase (7). The

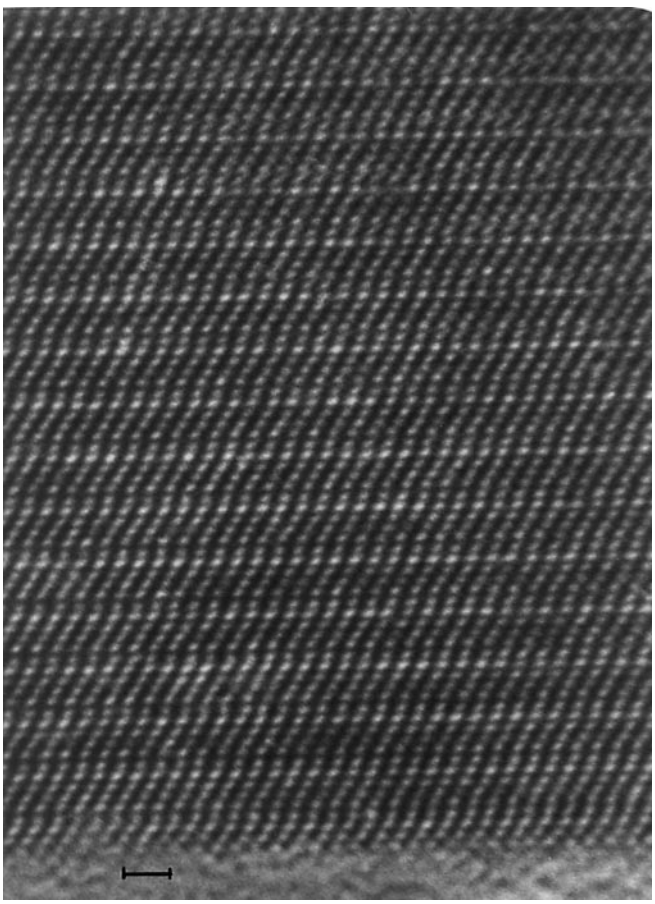

FIG. 1. Transmission electron microscope image (300 kV, C_s = 1.2 mm) viewed along [110] of H phase. The [001] direction is vertical. The scale bar corresponds to 10 Å.

image comprises slightly undulating rows of bright spots oriented along [4$\bar{4}$1]. The separation between the rows is 0.5 [1$\bar{1}$0]. Along the rows the image is repeated every fifth spot. Extended exposure of crystallites to the electron beam during the collection of images was observed to produce diffuse scattering in the selected area diffraction patterns, and was accompanied by a loss of long-range order in the images.

Development of a Structural Model

A structural model for the new phase was developed using a combination of crystal chemistry reasoning and information obtained from the TEM images. The unit cell parameters are consistent with a close-packed anion lattice, where the layer separation is $c/30 = 2.33$ Å and the anion–anion separation within the layers is $a/\sqrt{3} = 2.93$ Å. These distances are close to those found for example in rutile (distorted hexagonal close packed, *hcp*) or ilmenite, $FeTiO_3$ (*hcp*). Titanium has a strong preference for octahedral coordination. The location of titanium-occupied octahedral sites in the close-packed anion lattice was obtained directly from the TEM image shown in Fig. 1. For the defocus condition used of -1200 Å at the thin crystal edge, the bright spots correspond to projected high charge density, that is, to titanium atoms.

A schematic representation of the titanium atom distribution obtained from the TEM image is shown in Fig. 2. This diagram shows a 5-Å projection of all octahedral sites that occur in a *hcp* anion framework as small circles, with the proposed sites occupied by titanium shown as larger filled circles. The repeat distance along [001] of the titanium ordering is $15 \times 2.33 = 34.95$ Å, which is half of the *c* axis of the H1 phase. However the *hcp* anion lattice repeat along [001] is 2×2.33 Å, and so the true unit cell repeat is $30 \times 2.33 = 69.9$ Å to bring the anion and cation sublattices into coincidence.

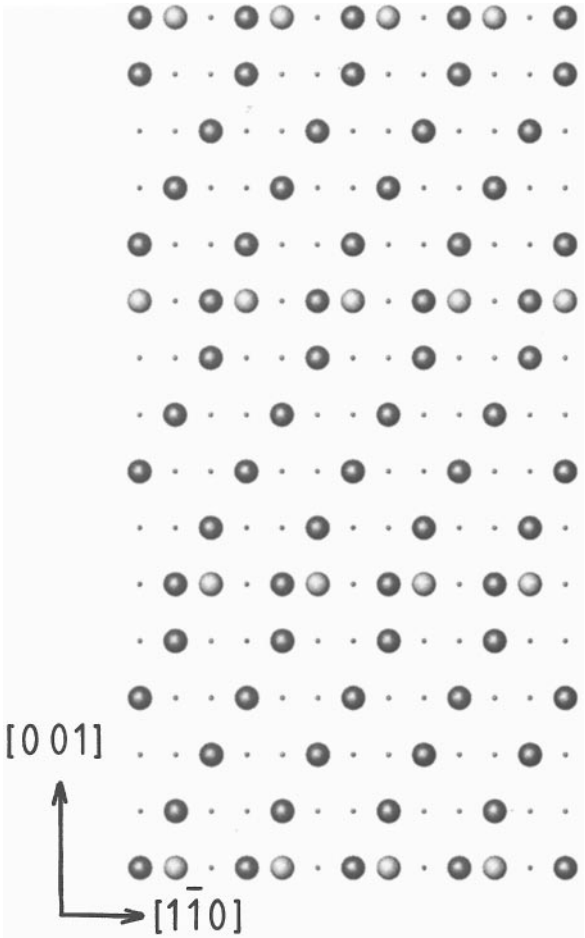

FIG. 2. 5-Å projection of all octahedral sites in a *hcp* oxygen array. Empty sites shown as small circles. Sites occupied by Ti in starting model shown by large dark-shaded circles. Ti atom subsequently located in structure analysis shown by large light-shaded circles.

Rietveld Refinement

The starting model for the Rietveld refinement was established in space group *R*3*c*. It comprised an ideal *hcp* oxygen lattice together with the titanium atom positions shown in Fig. 2. The 100 K XRD data set was used to refine the titanium and oxygen positions and to locate another titanium atom (shown by the light-shaded circles in Fig. 2) via difference Fourier syntheses. The ND data was then used to locate the lithium atoms and to further refine the oxygen atoms. The ND data was particularly useful for these purposes because of the strong scattering contrast between Ti, Li, Nb, and O with scattering lengths of -3.44, -1.90, 7.05, and 5.80 fm, respectively. A refinement of site occupancies indicated mixed occupancy of some sites. The results from the XRD and ND refinements were used in conjunction to establish the types of cation mixing, Ti/Li, Ti/Nb, and Li/Ti. The minor amount of rutile was included as a second phase in the refinements.

As the refinement progressed, it became evident that the atomic arrangement possessed a center of symmetry. The model was then redefined, with an appropriate origin shift, using the centrosymmetric space group $R\bar{3}c$. The final refinement of 33 profile parameters, coordinates, and group isotropic thermal parameters using the 1.5 K ND data (350 reflections) converged at $R_{wp} = 5.8\%$ and $R_B = 2.0\%$. The refinement using the 100 K XRD data (447 reflections) converged at $R_{wp} = 11.4\%$, $R_B = 2.5\%$ (12). The refined structural parameters from the two refinements are compared in Table 1. The higher *B* values obtained in the ND refinement are due to the high absorption cross-section of Li for neutrons (70.5 barns). The observed and calculated diffraction patterns from the Rietveld refinement of the ND data are given in Fig. 3.

TABLE 1
Results of Rietveld Refinement of ND Data[a] at 1.5 K and XRD Data[b] at 100 K

	Site and occupancy	x	y	z	B (Å^2)
Ti(1) ND	12*c*, Ti	$\frac{1}{3}$	$\frac{2}{3}$	0.0053(1)	0.45(1)
XRD		$\frac{1}{3}$	$\frac{2}{3}$	0.00484(1)	0.11(1)
Ti(2) ND	12*c*, Ti	$\frac{2}{3}$	$\frac{1}{3}$	0.0377(1)	0.45(1)
XRD		$\frac{2}{3}$	$\frac{1}{3}$	0.0374(1)	0.11(1)
Ti(3) ND	12*c*, 0.918(3) Ti	0	0	0.0674(2)	0.45(1)
XRD	+0.082 Nb	0	0	0.0676(1)	0.11(1)
Li(1) ND	12*c*, 0.970(2) Li	0	0	0.0287(2)	0.50(7)
XRD	+0.030 Nb	0	0	0.0282(1)	0.25(7)
Li(2) ND	12*c*, 0.850(4) Li	$\frac{1}{3}$	$\frac{2}{3}$	0.0583(1)	0.50(7)
XRD	+0.150 Ti	$\frac{1}{3}$	$\frac{2}{3}$	0.0596(1)	0.25(7)
Li(3)	12*c*, 0.50(2)Li	$\frac{2}{3}$	$\frac{1}{3}$	0.0866(1)	0.50(7)
		$\frac{2}{3}$	$\frac{1}{3}$	0.0867(1)	0.25(7)
O(1) ND	36*f*	−0.0220(5)	0.3643(5)	0.0163(1)	0.28(1)
XRD		−0.0214(7)	0.3678(8)	0.0159(1)	0.16(2)
O(2) ND	36*f*	0.3252(8)	0.2927(6)	0.0503(1)	0.28(1)
XRD		0.3255(9)	0.2919(7)	0.0505(1)	0.16(2)
O(3) ND	18*e*	0.6172(8)	0	$\frac{1}{4}$	0.28(1)
XRD		0.6174(9)	0	$\frac{1}{4}$	0.16(1)

[a] ND data, $T = 1.5$ K, $a = 5.0655(1)$ Å, $c = 69.7920(5)$ Å, $R_{wp} = 5.8\%$, $R_B = 2.0\%$.
[b] XRD data, $T = 100$ K, $a = 5.0668(1)$ Å, $c = 69.8302(2)$ Å, $R_{wp} = 11.4\%$, $R_B = 2.4\%$.

The unit cell composition of the H phase can be calculated from the starting composition, corrected for the amount of rutile in the product obtained from the Rietveld refinement (7.2 wt%). This gives a composition $Li_{28.5}Ti_{36.5}Nb_{1.1}O_{90}$. The composition can also be independently determined from the structure refinement using the refined site occupancies. The resulting composition, $Li_{27.8}Ti_{36.8}Nb_{1.3}O_{90}$, is in reasonable agreement with the rutile-corrected starting composition.

Description of Structure

A polyhedral representation of the structure of the H phase, projected along [110], is shown in Fig. 4. The diagram shows that the structure is an ordered intergrowth, parallel to (001), of blocks of corundum-type and $LiNbO_3$-type (LN) structures. The corundum part, $[Ti_2O_3]^{2+}$, of the intergrowth is centered on the metal atom layer containing Ti(1). The Ti(1)O_6 octahedra share edges within the (001) plane, and faces vertical to (001) as in Ti_2O_3. However Ti_2O_3 contains trivalent titanium and metal–metal bonding occurs across the shared octahedral face with Ti^{3+}–Ti^{3+} = 2.59 Å (16), whereas the H phase contains tetravalent titanium and strong repulsion occurs across the shared octahedral faces, giving Ti(1)–Ti(2) = 3.00 Å. This distance is considerably longer than the Ti^{4+}–Ti^{4+} distance of 2.69 Å across a shared octahedral face in 6H-$BaTiO_3$ (17). In the latter compound, Ti and Ba atoms stack along the hexagonal *c* axis and the shorter Ti-Ti distance is the result of a balance between Ti–O bonding forces and Ba–Ti nonbonded repulsions (18). In the corundum-type structure the Ti–Ti pairs are separated by vacant sites along the *c* axis,

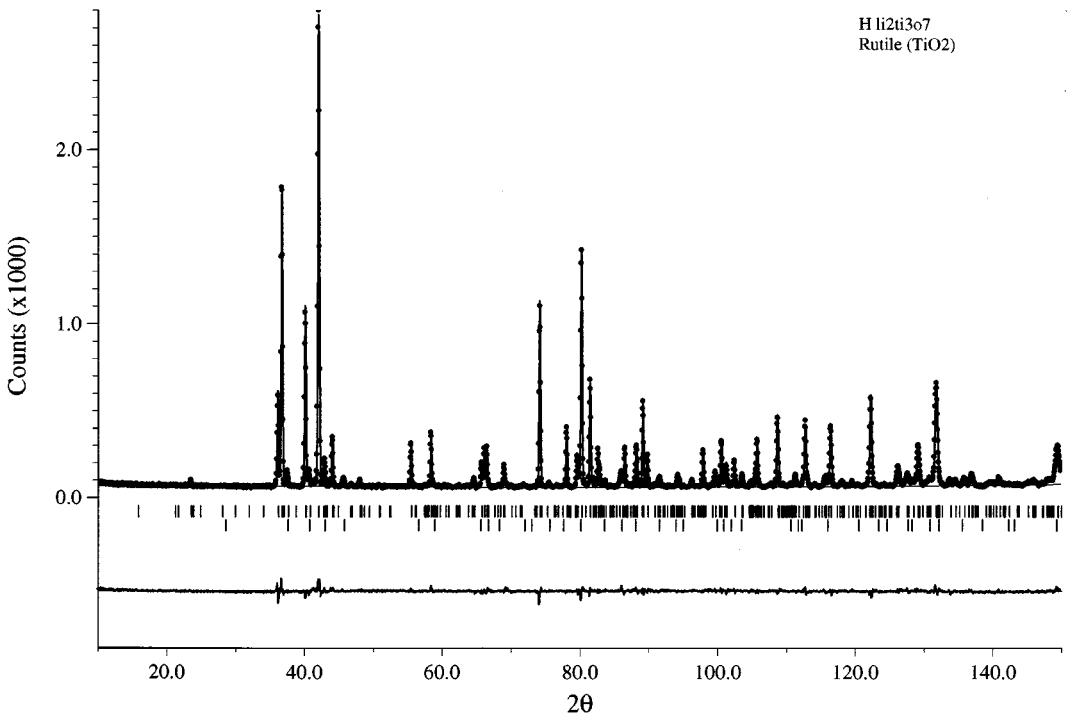

FIG. 3. Observed (dots), calculated (lines), and difference plots from Rietveld refinement of the 1.5 K neutron diffraction data. Bragg reflections for H phase and rutile shown.

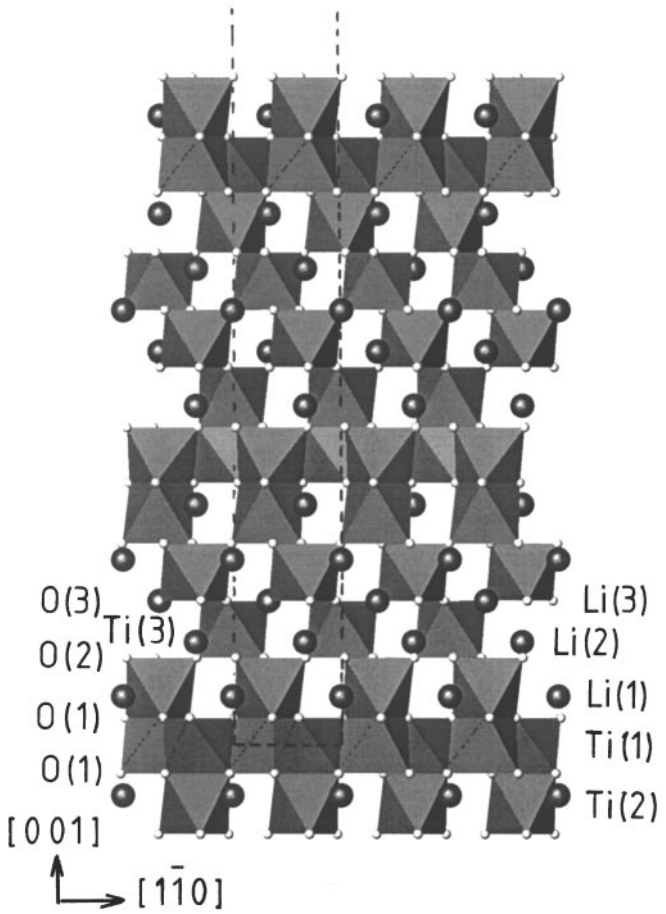

FIG. 4. Polyhedral representation of the structure of the H phase, projected along [110]. Filled circles correspond to Li.

and in the absence of metal–metal bonding, the structure is stabilized by large displacements of the metals toward the vacant sites. For example, in Fe_2O_3 the Fe–Fe distance is 2.89 Å (19).

The Ti_2O_3 segments are separated by blocks of $LiNbO_3$-type structure (20). At temperatures below 1470 K, LN is ferroelectric due to cooperative displacements along [001] of the Li and Nb atoms relative to the hexagonal close packed oxygen layers (21). In contrast, the centrosymmetric nature of the H phase structure results in the ferroelectric displacements of the metal atoms relative to the oxygen layers being of opposite polarity at either end of each block. In the middle of each block, a paraelectric region exists, where the Ti(3) atoms are located close to the midpoint between the oxygen layers. The different displacements of the metal atoms relative to the oxygen layers are shown in Fig. 5. As seen from Table 2, the Ti(2) atoms at the ends of the blocks have three short and three long Ti–O distances, 1.85 and 2.12 Å, as found for ferroelectric LN, while the Ti(3) atoms at the center of the blocks have relatively undistorted octahedra with Ti(3)–O distances of 1.93 and 1.97 Å.

In the central part of the LN-type blocks, the Li(3) atoms are strongly displaced to lie almost in the plane of the oxygen atoms, giving triangular coordination with Li(3)–O(3) = 1.95 Å and with three much longer Li(3)–O(2) distances of 2.64 Å. Bond valence calculations (22) give a reasonable calculated valence for Li(3), see Table 2. The geometry of the central part of the LN-type block is the same as observed in the paraelectric form of LN at temperatures above 1470 K (23). In particular, the oxygen atom O(3) takes up the special position $(x, 0, \frac{1}{4})$ and the Li(3) atom is disordered over two sites displaced along [001] by $\pm$ 0.23 Å from the plane of O(3) atoms.

The ND and XRD site occupancy refinements and valence sum calculations (Table 2) are consistent with a certain degree of cation mixing in the H phase. In particular the Li(2) site contains about 15% substitution by Ti. The occupation of Li(2) by Ti results in a localized region of corundum structure. The Nb dopant predominantly substitutes for Ti in the middle of the LN-type blocks. The site occupancy refinements were consistent with minor substitution of Nb also at the Li(1) site. However, this is more speculative because other schemes are possible involving all three cations and/or vacancies at the cation sites.

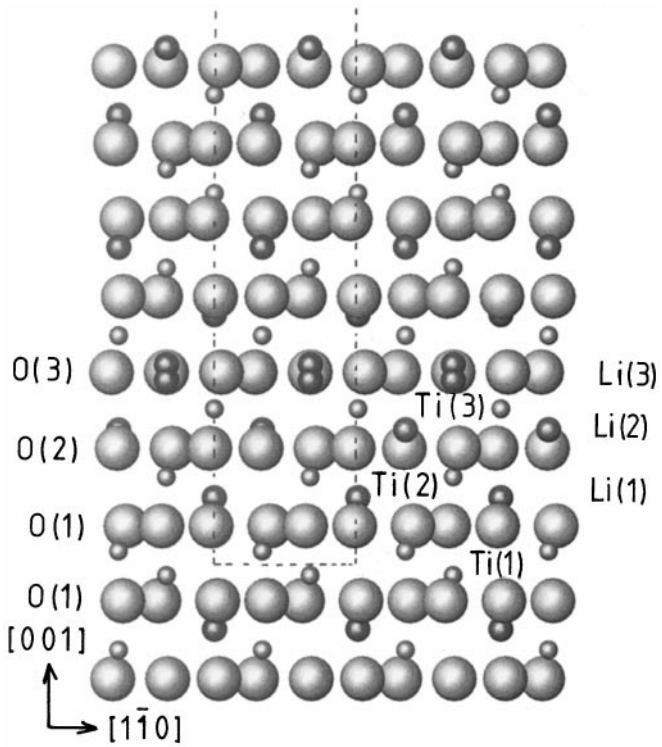

FIG. 5. [110] projection of the structure of the H phase, showing atomic positions. Large light circles are oxygen atoms, medium filled circles are Li, and smaller gray circles are Ti.

TABLE 2
Interatomic Distances (Å) from Refinements at 1.5 and 1173 K and Calculated Bond Valences[a]

	Data from ND refinement, 1.5 K		Data from XRD refinement, 1173 K	
	Distance	Bond valence (Ref. 22)	Distance	Bond valence
Ti(1)–O(1) × 3	1.85*	4.02	1.85	4.15
–O(1) × 3	2.13		2.09	
Ti(2)–O(2) × 3	1.86	3.99	1.89	3.94
–O(1) × 3	2.12		2.16	
Ti(3)–O(3) × 3	1.93	4.15	1.94	4.16
–O(2) × 3	1.97		1.96	
Li(1)–O(1)	2.09	0.99	2.18	0.83
–O(2)	2.18		2.22	
Li(2)–O(2)	1.96	1.07	2.05	0.92
–O(3)	2.35		2.32	
Li(3)–O(3)	1.95	0.93	1.97	0.88
–O(2)	2.64		2.65	
Ti(1)–Ti(1) edge	3.02		3.03	
–Ti(2) face	3.00		2.98	
Ti(2)–Li(1) edge	2.99		3.04	
–Li(3) none	2.95		2.98	
Ti(3)–Li(1) face	2.70		2.80	
–Li(2) face	2.86		2.77	
–Li(2) edge	2.99		3.02	
–Li(3) corner	3.05		3.08	

[a] Errors associated with M–O and M–M are in the range 0.01–0.02 Å.

Structure Changes with Temperature

The results of Rietveld refinements of the powder XRD data at temperatures of 303, 473, 673, 873, 1073, and 1173 K are given in Table 3. Both a and c parameters vary linearly with temperature in this range. The cell expansion is almost isotropic with $\alpha(a) = 13.2 \times 10^{-6}\,K^{-1}$ and $\alpha(c) = 12.6 \times 10^{-6}\,K^{-1}$. This contrasts with the highly anisotropic expansion of ferroelectric LN for which $\alpha(a) = 16.7 \times 10^{-6}\,K^{-1}$ and $\alpha(c) = 2 \times 10^{-6}\,K^{-1}$ (21). The isotropic displacement parameters for Ti, Li, and O show linear dependences on temperature, with a deviation toward higher values for O at temperatures above 873 K.

The major structural responses to increase in temperature, apart from the isotropic unit cell expansion, are rotations of the oxygen atoms O(2) and O(3) about the 3-fold axes. The effect of these rotations is to increase the separation of the triangular groupings of oxygens bonded to Li and to decrease the separation of the triangular groupings bonded to Ti. The latter effect counteracts the lattice expansion and as a consequence the size of the $Ti(1)O_6$ and $Ti(3)O_6$ octahedra remain essentialy unchanged with increasing temperature (a correction for anisotropic thermal motion of the oxygens would probably eliminate the observed small contraction). The polyhedral bond distances at temperatures of 1.5 and 1173 K are compared in Table 2.

The largest bond length changes with temperature are associated with $Li(1)O_6$ and $Li(2)O_6$ (see Table 2). The inability to satisfy the valence requirements of Li as the temperature is increased may well be the driving force for the decomposition of the H phase (to rutile plus spinel and then to the R phase) at temperatures above 1230 K (8).

R Phase to H Phase Transformation

The R phase of lithium titanate, $Li_{1.72}[Li_{0.57}Ti_{3.43}]O_8$, has orthorhombic symmetry *Pnma*, with $a = 9.542$ Å,

TABLE 3
Results of Rietveld Refinements of Powder XRD Data at Different Temperatures

	303 K	473 K	673 K	873 K	1073 K	1173 K
a (Å)	5.0744(1)	5.0849(1)	5.0984(1)	5.1121(1)	5.1260(1)	5.1329(1)
c (Å)	69.9405(3)	70.0790(3)	70.2531(3)	70.4275(3)	70.6122(3)	70.7088(3)
z, Ti(1)	0.0048(1)	0.0048(1)	0.0047(1)	0.0046(1)	0.0045(1)	0.0044(1)
z, Ti(2)	0.0375(1)	0.0375(1)	0.0375(1)	0.0376(1)	0.0377(1)	0.0378(1)
z, Ti(3)	0.0676(1)	0.0677(1)	0.0678(1)	0.0678(1)	0.0678(1)	0.0679(1)
B Ti (Å^2)	0.32(1)	0.56(1)	0.76(1)	0.97(1)	1.22(1)	1.39(2)
z, Li(1)	0.0283	0.0283	0.0283	0.0283	0.0283	0.0283
z, Li(2)	0.0596	0.0596	0.0596	0.0596	0.0596	0.0596
z, Li(3)	0.0867	0.0867	0.0867	0.0867	0.0867	0.0867
B, Li (Å^2)	0.90(7)	1.24(7)	1.66(8)	1.99(8)	2.36(9)	2.7(1)
x, O(1)	− 0.0217(7)	− 0.0224(7)	− 0.0207(7)	− 0.0214(7)	− 0.0204(8)	− 0.0180(8)
y, O(1)	0.3679(8)	0.3691(8)	0.3708(9)	0.3722(9)	0.375(1)	0.379(1)
z, O(1)	0.0159(1)	0.0158(1)	0.0158(1)	0.0157(1)	0.0157(1)	0.0159(1)
x, O(2)	0.3256(9)	0.3258(9)	0.324(1)	0.324(1)	0.322(1)	0.320(1)
y, O(2)	0.2899(7)	0.2889(8)	0.2854(8)	0.2839(8)	0.2812(9)	0.279(1)
z, O(2)	0.0505(1)	0.0506(1)	0.0507(1)	0.0508(1)	0.0510(1)	0.0508(1)
x, O(3)	0.618(1)	0.618(1)	0.618(1)	0.616(1)	0.619(1)	0.618(1)
B, O (Å^2)	0.36(2)	0.62(3)	0.93(3)	1.15(3)	1.53(3)	1.73(4)
R_{wp} (%)	11.7	11.6	11.3	10.8	11.3	12.5
R_B (%)	2.5	2.6	2.6	2.8	2.5	2.7

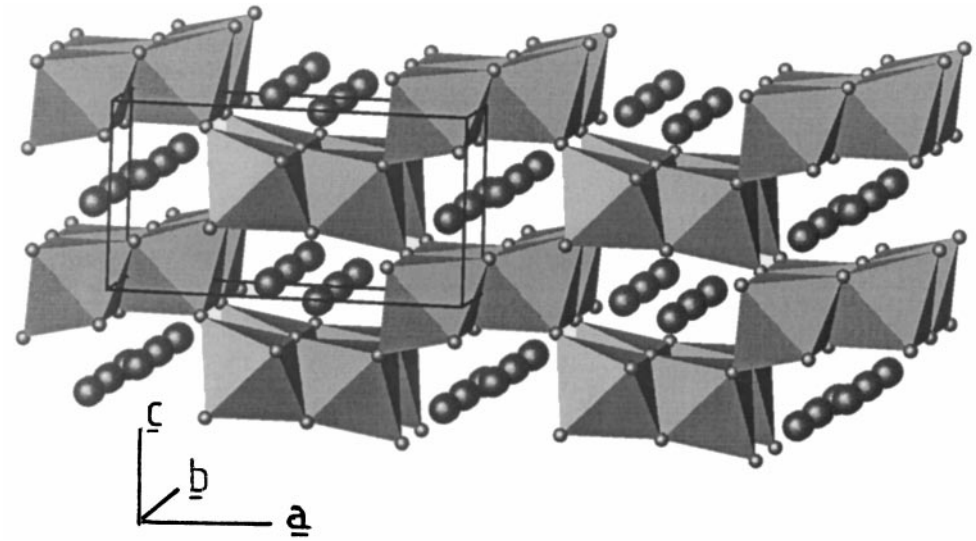

FIG. 6. Polyhedral representation of the ramsdellite form of lithium titanate. Filled circles are Li atoms.

$b = 2.944$ Å, and $c = 5.014$ Å (24). The structure, shown in Fig. 6, comprises a distorted hexagonal close-packed oxygen framework with ordering of Ti atoms into octahedral sites to form double chains of edge-shared octahedra along [010]. The double chains are interconnected to equivalent chains in adjacent (001) layers via corner sharing, creating $[2 \times 1]$ channels. Three-quarters of the Li atoms occupy tetrahedral sites in the channels, with the remaining 25% substituting for Ti in the octahedra, as indicated by the formula above.

The R phase is stable only at temperatures above 1213 K, below which it decomposes to a mixture of rutile plus spinel (5, 6). However quenching from above 1213 K preserves the R phase at ambient conditions. When this metastable R phase is heated above 800 K, it slowly transforms to the H phase. Our structure determination of the H phase shows that this transformation involves extensive diffusion and relocation of Li and Ti atoms within the *hcp* oxygen framework, which results in a modulation of the cation composition normal to the close-packed layers. In the R phase each (001) layer has the same average composition, i.e., $Ti_{1.29}Li_{0.86}O_3$ (relative to 3 oxygens for ease of comparison with the H phase). In the H phase, ignoring the minor niobia substitution, the composition varies from $[Ti_2O_3]^{+2}$ in the corundum-type layer through $[Ti_{1.03}Li_{0.97}O_3]^{-0.9}$ in the LN-type layers to $[Ti_{1.14}Li_{1.35}O_3]^{-0.1}$ in the paraelectric LN-type layers. Thus relative to the R phase there is a modulation between Ti-rich and Li-rich layers in the H phase, where the modulation period is 2.5 times the *c* axis periodicity of the R phase, i.e., 5 cation layers. Associated with this composition modulation is a formal charge separation as indicated by the charges assigned to each layer above. However, the structure adjusts to this charge imbalance by local atomic displacements so that the calculated valence sums at the different cation sites are close to the expected values at low temperatures, as shown by the results in Table 2. As the H phase is heated the combined effects of thermal expansion and oxygen displacements progressively make it more difficult for the lithium to satisfy its valence requirements. Ultimately the phase separation becomes complete when the H phase is heated above 1230 K and it decomposes into TiO_2 (rutile) and $Li_4Ti_5O_{12}$ (spinel), before reforming the R phase (8).

The reported beneficial role of added niobia in stabilizing the H phase (8) can now be understood in terms of its stabilization of the $LiNbO_3$-type structure element. It is interesting to compare the unit cell dimensions of the niobia-doped H and R phases. This comparison can be made readily by taking the orthohexagonal oxygen subcells for both phases. Tsubone and Shimizu (8) have reported the change in unit cell dimensions of the R phase with addition of niobia. Relatively large cell parameter increases were observed for additions of up to about 1 mol% of Nb_2O_5, after which the parameters remained almost unchanged at $a = 9.566$ Å, $b = 2.950$ Å, and $c = 5.032$ Å, using the P*nma* space group orientation. The corresponding orthohexagonal parameters for the oxygen subcell are $a = 4.783$ Å, $b = 2.950$ Å, and $c = 5.032$ Å. The subcell parameters for the niobia-doped H phase at ambient can be calculated from the parameters in Table 3, giving $a = 5.074$ Å, $b = 2.929$ Å, and $c = 4.663$ Å. The R to H phase transformation thus involves a large anisotropic expansion within the close-packed layers and a large contraction of the separation between the layers. This is due essentially to a flattening of the anion layers in the H phase, which are strongly puckered along [100] in the R phase in order to

accomodate the Li atoms in tetrahedral interstices in the channels (24).

The ambient temperature subcell parameters correspond to a 2.4% volume contraction in going from the R to the H phase. The linear expansion coefficient for the R phase has been reported to be $12.5 \times 10^{-6}\ K^{-1}$(8), which is close to the value that we measured for the H phase, so a similar volume contraction is expected at the transformation temperature. Thus there is a density increase on going from the R phase to the H phase which is consistent with the increase in coordination number for the majority of the Li atoms from 4 to 6.

CONCLUSIONS

The ramsdellite form of lithium titanate, $Li_{1.72}[Li_{0.57}Ti_{3.43}]O_8$, is unstable below 1213 K but can be retained metastably by quenching. When the quenched R phase is reheated slowly to above $\sim$800 K it transforms to a new polymorph with trigonal symmetry, which has become known in the literature as the H phase. Pre-doping of the R phase with niobia stabilizes the H phase against decomposition to rutile plus spinel.

We have determined and refined the structure of the H phase stabilized with 4 mol % niobia by combining TEM studies with Rietveld analysis using both XRD and ND powder data. The structure can be described as an ordered intergrowth, parallel to (001), of corundum-type Ti_2O_3 blocks with $LiNbO_3$-type blocks. The LN-type blocks contain elements of both ferroelectric and paraelectric LN-type structure elements.

The structural evolution of the H phase has been studied as a function of temperature using powder XRD data collected between 1.5 and 1173 K. With increasing temperature the oxygen atoms rotate about the 3-fold axes to counteract the unit cell expansion and maintain the size of the TiO_6 octahedra relatively constant. This results in large increases in the Li–O bond lengths, with an eventual destabilisation of the H phase relative to a mixture of rutile plus spinel at a temperature of $\sim$1230 K.

ACKNOWLEDGMENTS

We thank the ESRF, Grenoble, for beam time allocation and Eric Dooryhee for help in setting up the experiments at BM16, ESRF. I.E.G. thanks the Université Joseph Fourier and the CNRS Laboratoire de Cristallographie for support during his visit to Grenoble.

REFERENCES

1. G. H. Jonker, *Trab. Reun. Int. React. Solidos, Madrid* 413 (1957).
2. M. Lundberg and S. Andersson, *Acta Chem. Scand.* **18,** 817 (1964).
3. B. Morosin and J. C. Mikkelsen, *Acta Crystallogr. Sect. B* **35,** 798 (1979).
4. R. S. Roth, H. S. Parker, and W. S. Brower, *Mater. Res. Bull.* **8,** 327 (1973).
5. G. Izquierdo and A. R. West, *Mater. Res. Bull.* **15,** 1655 (1980).
6. J. C. Mikkelsen, Jr., *J. Am. Ceram. Soc.* **63,** 331 (1980).
7. J. Zou, F. H. Li, D. Y. Yang, Y. D. Jiang, and K. H. Kuo, *Phil. Mag. B* **57,** 103 (1988).
8. D. Tsubone and T. Shimizu, *J. Ceram. Soc. Jpn., Int. Ed.* **101,** 637 (1993).
9. W. K. Collins, W. D. Riley, and B. W. Jong, *EPD Congress 1993* (J. P Hager, Ed.), 419 (1992).
10. A. N. Fitch, *IUCr Commun. Powder Diff. Newslett.* **17,** 1 (1996).
11. A. W. Hewatt, *Chem. Scr.* **26A,** 119 (1986).
12. R. J. Hill and C. J. Howard, Australian Atomic Energy Commission (now ANSTO) Report No. M112. Lucas Heights Research Laboratories, NSW, Australia, 1986.
13. D. B. Wiles and R. A. Young, *J. Appl. Crystallogr.* **14,** 149 (1981).
14. J. Rodriguez-Carjaval, "Collected Abstracts of Powder Diffraction Meeting," Vol. 127 Toulouse, France, 1990.
15. G. Cagliotti, A. Paoletti, and F. P. Ricci, *Nucl. Instrum.* **3,** 223 (1958).
16. R. E. Newnham and Y. M. de Haan, *Z. Kristallogr.* **117,** 235 (1962).
17. J. Akimoto, Y. Gotoh, and Y. Oosawa, *Acta Crystallogr. Sect. C* **50,** 160 (1994).
18. I. E. Grey, C. Li, L. M. D. Cranswick, R. S. Roth, and T.A. Vanderah, *J. Solid State Chem.* **135,** 312 (1998).
19. D. A. Perkins and J. P. Attfield, *J. Chem. Soc., Chem. Commun.* 229 (1991).
20. H. D. Megaw, *Acta Crystallogr. Sect. A* **24,** 583 (1968).
21. S. C. Abrahams, H. J. Levinstein, and J. M. Reddy, *J. Phys. Chem. Solids* **27,** 1019 (1966).
22. N. E. Brese and M. O'Keeffe, *Acta Crystallogr. Sect. B* **47,** 192 (1991).
23. H. Lehnert, H. Boysen, F. Frey, A. Hewatt, and P. Radaelli, *Z. Kristallogr.* **212,** 712 (1997).
24. I. Abrahams, P. G. Bruce, W. I. F. David, and A. R. West, *J. Solid State Chem.* **78,** 170 (1989).